


Spectroscopic Evidence for Lactam Formation in Terminal Ornithine b_2^+ and b_3^+ Fragment Ions

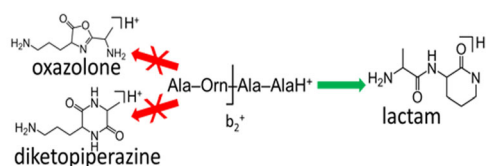
Zachary M. Smith,¹ Xiye Wang,¹ Jonathan R. Scheerer,¹ Jonathan Martens,² Giel Berden,² Jos Oomens,² Vincent Steinmetz,³ Arpad Somogyi,⁴ Vicki Wysocki,⁴ John C. Poutsma¹ 

¹Department of Chemistry, The College of William & Mary, Williamsburg, VA 23187-8795, USA

²Institute for Molecules and Materials, FELIX Laboratory, Radboud University, Nijmegen, The Netherlands

³Laboratoire de Chimie Physique, CNRS UMR 8000, Université Paris, 91405, Orsay, France

⁴Department of Chemistry and Biochemistry, The Ohio State University, Columbus, OH 43210-1173, USA



Abstract. Infrared multiple photon dissociation spectroscopy was performed on the AlaOrn b_2^+ and AlaAlaOrn b_3^+ fragment ions from ornithine-containing tetrapeptides. Infrared spectra were obtained in the fingerprint region (1000–2000 cm^{-1}) using the infrared free electron lasers at the Centre Laser Infrarouge d’Orsay (CLIO) facility in Orsay, France, and the free electron lasers for infrared experiments (FELIX) facility in Nijmegen, the Netherlands. A novel terminal or-

nithine lactam $\text{AO}^+ b_2^+$ structure was synthesized for experimental comparison and spectroscopy confirms that the b_2^+ fragment ion from AOAA forms a lactam structure. Comparison of experimental spectra with scaled harmonic frequencies at the B3LYP/6-31+G(d,p) level of theory shows that $\text{AO}^+ b_2^+$ forms a terminal lactam protonated either on the lactam carbonyl oxygen or the N-terminal nitrogen atom. Several low-lying conformers of these isomers are likely populated following IRMPD dissociation. Similarly, a comparison of the experimental IRMPD spectrum with calculated spectra shows that $\text{AAO}^+ b_3^+$ -ions also adopt a lactam structure, again with multiple different protonation sites, during fragmentation. This study provides spectroscopic confirmation for the lactam cyclization proposed for the “ornithine effect” and represents an alternative b_n^+ structure to the oxazolone and diketopiperazine/macrocycle structures most often formed.

Keywords: IRMPD spectroscopy, b_2^+ ions, Peptide fragmentation

Received: 6 December 2018/Revised: 24 April 2019/Accepted: 26 April 2019/Published Online: 10 June 2019

Introduction

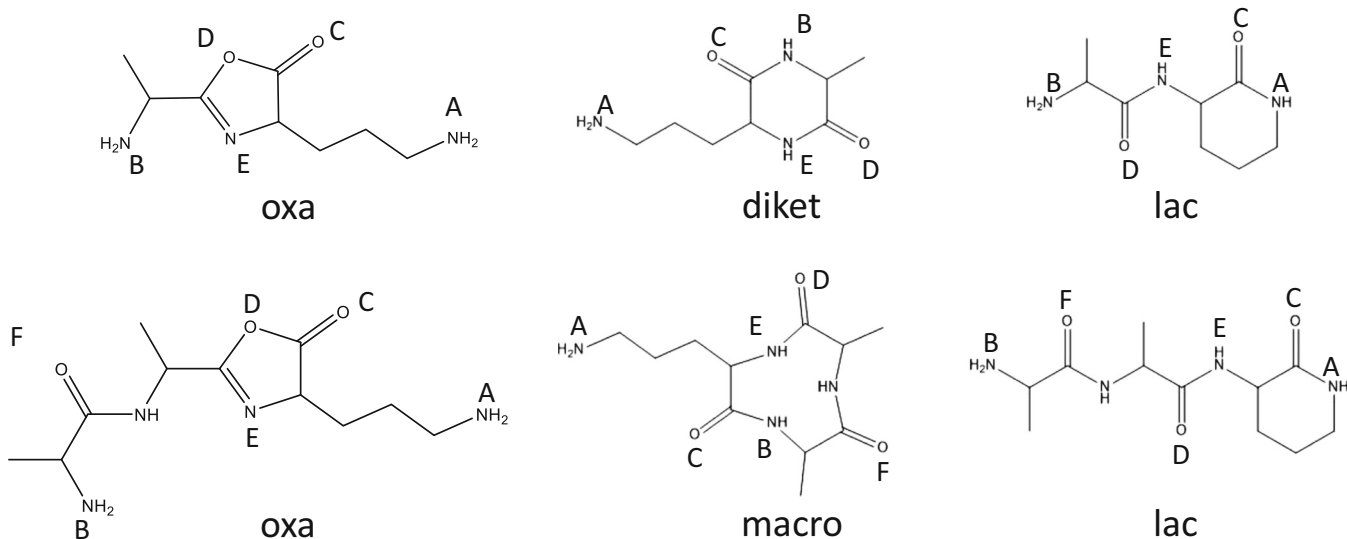
Structural identification at the molecular level yields insight into the function of biochemically active species. While condensed-phase techniques have served as reliable standards for determining structure, the introduction of soft ionization techniques—such as MALDI and ESI—has catalyzed the mass spectrometer’s ability to identify these species in the gas phase

[1–3]. Soft ionization has brought about a method for the reliable sampling of biological systems ranging in size from individual amino acids to large protein complexes in reproducible charge states and conformations. Gas-phase analysis of these systems probes the intrinsic energetics and interactions adopted by the structure thereby avoiding changes induced by solvent interaction.

Structural identification of peptides and their fragments is a focus of proteomics-related mass spectrometry research. Due to their ubiquity in collision-induced dissociation (CID) and infrared multiple photon dissociation (IRMPD) pathways, the formation, and structure of b-type ions are of particular interest to these studies [4–21]. Until now, two major pathways have been documented for the smallest multiple-residue b-ion system,

Electronic supplementary material The online version of this article (<https://doi.org/10.1007/s13361-019-02244-0>) contains supplementary material, which is available to authorized users.

Correspondence to: John Poutsma; e-mail: jcpout@wm.edu



Scheme 1. The protonation sites explored computationally for the oxazolone (left), diketopiperazine/macrocyclic (middle), and lactam (right) for AO⁺ b₂⁺ and AAO⁺ b₃⁺.

b₂⁺. An oxazolone structure is formed from nucleophilic attack of the first residue's carbonyl oxygen on the second residue's carbonyl carbon (see Scheme 1) [4]. A diketopiperazine structure is formed by nucleophilic attack of the N-terminus on the second residue carbonyl carbon (see Scheme 1) [4]. For most residues, the diketopiperazine structure is lower in energy but requires a *trans-cis* isomerization of the peptide bond in order to form [4]. Consequently, the majority of b₂⁺ ions that have been characterized spectroscopically are oxazolones [6–9, 11, 12, 15–18, 21]. Alternative fragmentation pathways have been proposed involving the side chains of specific residues containing heteroatoms such as glutamine and asparagine [19, 22], histidine [23], arginine [4, 24], and lysine [4]. A lactam structure has been proposed to occur from nucleophilic attack of an amino side chain on its own carbonyl (Arg, Lys, Orn, His) [4].

Previous studies have investigated the effects of side-chain influence on fragmentation. McLuckey and co-workers identified preferential b-ion formation C-terminal to ornithine (Orn) residues—dubbed the ornithine effect—and presented fragmentation patterns consistent with a terminal lactam b-ion structure [25]. Subsequent work has exploited this effect in the development of analytical techniques to probe cyclic and stapled peptides, thereby providing fragments of known lengths for sequencing [26]. Confirmation of this terminal Orn b-ion structure will provide insight into available fragmentation pathways, and will be instructive in identifying similar mechanisms in peptides containing other amino acids with heteroatoms on their side chains.

Gas-phase structural validation can be performed by a variety of mass spectrometric techniques including fragmentation studies, isotope labeling, hydrogen-deuterium exchange, and ion mobility. A more recent approach to structural identification is through the use of ion infrared spectroscopy and

computational calculations. Infrared multiple photon dissociation (IRMPD) action spectra can provide spectroscopic evidence for the structure of fragment ions [27]. While IRMPD studies have provided spectroscopic evidence for the diketopiperazine [9, 11, 15, 20] and oxazolone [6, 7, 11, 12, 15, 16] pathways, the potential lactam pathway has not been probed spectroscopically. In the present work, we compare IR spectra of the AO⁺ b₂⁺ and AAO⁺ b₃⁺ fragment ions to their theoretically predicted IR spectra and present spectroscopic evidence for the lactam b-ion pathway.

Experimental and Theoretical Methods

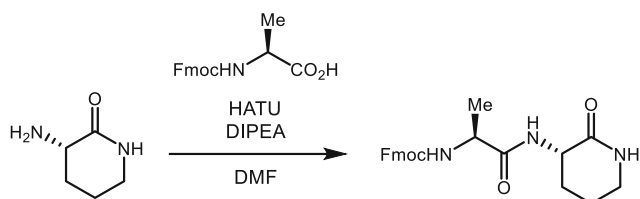
Materials

Alanine Wang resin was purchased from ChemPep Inc. (Wilmington, FL). Fmoc-Alanine-OH and Fmoc-Ornithine(BOC)-OH were purchased from MilliporeSigma (Burlington, MA). (S)-3-amino-2-piperidone was purchased from Sigma-Aldrich (Burlington, MA). All materials were used without purification.

Solid-phase reactions were carried out in disposable 12-ml plastic fritted syringes. Solution-phase reactions were carried out under an atmosphere of nitrogen in flame-dried or oven-dried glassware with magnetic stirring unless otherwise indicated. Silica-bound piperazine (0.93 mmol/g loading) was purchased from Silicycle Inc. (product number R60030B).

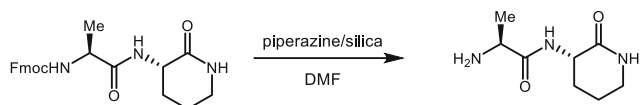
Synthetic Procedures

Tetrapeptides AOAA and AAOA were synthesized using standard Fmoc—solid state peptide synthesis protocols described elsewhere [28, 29]. An authentic AO⁺ b₂ lactam was synthesized according to the following procedures:



(9H-Fluoren-9-yl)Methyl ((S)-1-oxo-1-(((S)-2--Oxopiperidin-3-yl)Amino)Propan-2-yl)Carbamate

A dry flask was charged with (S)-3-aminopiperidin-2-one (50 mg, 0.438 mmol) and dissolved in dimethyl formamide (DMF, 2 mL). (((9H-fluoren-9-yl)methoxy)carbonyl)-L-alanine (136 mg, 0.438 mmol), diisopropylethylamine (DIPEA, 57 mg, 0.438 mmol), hexafluorophosphate azabenzotriazole tetramethyl uronium (HATU, 333 mg, 0.876 mmol) were added to the flask. The reaction was stirred overnight and diluted with EtOAc (20 mL). The solution was washed with saturated NH₄Cl (20 mL), and saturated NaHCO₃ (20 mL). The organic layer was dried with anhydrous Na₂SO₄ and concentrated in vacuo. The resulting peptide product (quantitative yield) was obtained as a white solid, and was used without further purification: ¹H NMR (400 MHz, CD₃OD) 1.31 (m, 4H), 1.46–2.06 (m, 2H), 3.19 (m, 1H), 3.67 (m, 2H), 3.95–4.25 (m, 2H), 4.33 (m, 2H), 7.32 (m, 5H), 7.65 (m, 2H), 7.77 (m, 2H), 7.97 (s, 1H) (Figure S1 of supporting information). ¹H NMR spectra were recorded on a Varian Mercury 400 (400 MHz) spectrometer and are reported in ppm using tetramethylsilane (0.00 ppm).



(S)-2-Amino-N-((S)-2-Oxopiperidin-3-yl)Propenamide

A dry flask was charged with (9H-fluoren-9-yl)methyl ((S)-1-oxo-1-(((S)-2-oxopiperidin-3-yl)amino)propan-2-yl)carbamate (56 mg, 0.137 mmol) and dissolved in DMF (2.8 mL). Silica-immobilized piperazine (1.48 g, 1.374 mmol) was added to the flask and the reaction was stirred overnight. The reaction mixture was then filtered through a pad of celite, washed with MeOH, and concentrated in vacuo. The resulting white solid (19 mg) contained both the desired peptide product and some untrapped methylene fluorene (30% by crude NMR). This material was used for MS spectroscopic analysis without further purification: Data for peptide product: ¹H NMR (400 MHz, CD₃OD) 1.28 (m, 2H), 1.44 (d, J = 7 Hz, 3H), 1.59 (m, 1H), 1.86 (m, 1H), 3.23 (m, 2H), 3.43 (m, 1H), and 4.04 (m, 1H) (Figure S2 of supporting information).

Experimental Methods

Infrared multiphoton dissociation spectra were obtained at the free electron laser for infrared experiments (FELIX) [30, 31] facility in Nijmegen, Netherlands, and at the Centre Laser Infrarouge d'Orsay in Orsay, France [32, 33].

FELIX

The infrared vibrational spectrum for AO⁺ b₂⁺ was obtained as an IRMPD action spectrum. A dilute solution (~1 μM) of AOOA was prepared in acidified (~1% formic acid) 50:50 CH₃CN:H₂O and directly injected into a modified Bruker amaZon ion trap mass spectrometer via an electrospray ionization source. Mass spectrometer conditions and ion focusing optics were tuned to optimize the signal for the protonated AOOA ion. This ion was mass-selected and allowed to undergo CID fragmentation with the background helium gas (pressure ~10⁻³ mbar) to yield the corresponding b₂⁺ ion. Ion focusing and collision-induced dissociation conditions were varied in order to maximize the production of the b₂⁺ product ion. Typical isolation and accumulation times were ~40 ms. The b₂⁺ “precursor” ion was then mass-selected and irradiated with infrared radiation from the FEL. Isolation conditions were adjusted in order to ensure that only *m/z* 186 was present in the trap (unit mass resolution). The IRMPD fragment intensities were monitored as the wavelength is scanned. An infrared spectrum was generated by plotting the sum of all fragment ions normalized to the sum of the fragments and the precursor ion (Σ (fragments) / Σ (fragments + precursor)). Similar procedures were used for the authentic protonated lactam species, with the exception of the CID fragmentation step. Ion focusing conditions were adjusted to maximize the signal for *m/z* 186, again with unit mass resolution.

The FELIX FEL operates at a 1-GHz macropulse with 10 Hz micropulses. Optical sensors detect the firing laser and open shutters to the ion trap chamber for 200 ms, irradiating trapped ions with 2 pulses of the laser. The laser moves in steps of ~4 cm⁻¹, and six averages are taken at each measured wavelength. Wavelength validation occurs online via a grating spectrometer, and an additional correction takes place during data work up from power and wavelength calibrations taken between runs. The difference in expected and reported wavelengths is fit to the expected wavelength as a polynomial function such that no point varies from the fit by more than 0.02 μm, the limit of detection for the spectrometer. This polynomial fit is applied to the wavelengths scanned, and then converted to wavenumbers for use in captured spectra. A correction for frequency-dependent laser power variation is also applied during data workup.

CLIO

Similar procedures were used to obtain an IRMPD spectrum for AAO⁺ b₃⁺ ion from protonated AAOA. The modified Bruker Esquire instrument required a higher concentration (~10 mM) of peptide and acidified 50:50 H₂O:MeOH was used as the solvent. Ion source and mass spectrometer-focusing conditions were adjusted to optimize the formation of the protonated AAOA ion. As with the AO⁺ b₂⁺ ion, collision-induced dissociation with the background helium gas (pressure

$\sim 10^{-3}$ mbar) was used to generate the AAO⁺ b₃⁺ precursor ion. Isolation and fragmentation conditions were optimized in order to maximize the production of the AAO⁺ b₃⁺ ion at *m/z* 257, with typical isolation and accumulation times of ca. 100 ms. The AAO b₃⁺ fragment ion is re-isolated in MS³ and allowed to interact with the tuned IR light of the FEL for 200 ms. An average of four individual fragmentation experiments is taken at each laser wavelength.

The FEL output consists of 8 μ s macropulses at 25 Hz. The macropulse energy is ca. 20 mJ. The laser wavelength is varied in ca. 6 cm⁻¹ steps and the laser bandwidth is about 0.3–0.5% of the center wavelength. FEL wavelength calibration occurs at CLIO by splitting the beam and passing a portion through a polystyrene film as a control spectrum in real time. This experimental spectrum is then linearly fit to a known polystyrene spectrum. This linear fit is applied to the analyte as a wavelength correction. The power (mJ) at each wavelength is also measured and is fit to the wavelength as a polynomial function. The measured intensity is then divided by the normalized power to produce the corrected absorbance. Final analyte spectra are then normalized and have a three-point average smoothing factor applied.

Theoretical Procedures

Calculations for the lactam, diketopiperazine/macrocyclic, and oxazolone isomers of AO⁺ and AAO⁺ were computed using the Gaussian 09 suite of programs [34]. Conformer sets were generated for several protonation sites (see Scheme 1) using the GMMX searching routine in PCModel 9 that varies dihedral angles, saving structures with energies within 40 kJ/mol of the minimum energy structure [35]. These conformer sets were imported into Gaussian 09 and used as starting structures for a series of molecular orbital and density functional theory calculations. Conformers with redundant energies were removed from the conformer sets. Final geometries, zero-point energies (ZPE), and thermal corrections to free energy were computed at the B3LYP/6-31+G(d) level of theory for all species [36, 37].

Naming of the conformer types follows the convention of the isomer name followed directly by a letter corresponding to the protonation site (A: Orn side chain nitrogen atom (b₂⁺ and b₃⁺), B: N-terminal Ala nitrogen atom (b₂⁺ and b₃⁺), C: C-terminal Orn carbonyl oxygen atom (b₂⁺ and b₃⁺), D: preceding Ala carbonyl oxygen atom (b₂⁺ and b₃⁺), E: backbone nitrogen atom of Orn residue (b₂⁺ and b₃⁺), and F: carbonyl oxygen atom of first Ala residue (b₃⁺ only)). Diketopiperazine has been shortened to diket, macrocyclic has been shortened to macro, oxazolone has been shortened to oxa, and lactam has been shortened to lac. All optimized structures were assigned to one of the isomer subtypes and were given a number based on relative free energy (e.g., *oxaA_001*) at the B3LYP/6-311++G(d,p)//B3LYP/6-31+G(d) level of theory. Structures for the lowest-energy conformer for the different protomers of the lac, diket, and oxa isomers of AO⁺ b₂⁺ are shown in Figure 1 and those for AAO⁺ b₃⁺ are shown in Figure 2.

Free energies were derived by extracting the total electronic energy from a single-point energy calculation at the B3LYP/6-311++G(d,p) level of theory and converting to 298K free energy using the B3LYP/6-31+G(d)-computed thermal correction. The recommended scaling factors for ZPE and integrated heat capacities for B3LYP-derived frequencies are 0.98 and 0.99, respectively [38]. Due to the small differences between the recommended scaling factors and the unscaled harmonic frequencies, we chose to use the unscaled harmonic frequencies to derive ZPE and thermal corrections. This combination of triple-zeta single-point energy calculations at double-zeta geometries has been shown to give predictions for proton affinities for a variety of amino acids and other nitrogen-containing compounds that are in excellent agreement with experimental determinations from our lab [39–42].

Computed relative free energies at 298 K are tabulated for all low-lying (< 25 kJ/mol above lowest-energy structure) conformers of the *lacB*, *lacC*, *lacD*, and *diketA* isomers of AO⁺ b₂⁺ in Table 1. The free energies for the lowest-energy conformer of the higher-energy isomers (*lacA*, *lacE*, *diketC*, *diketD*, *oxaA*, *oxaB*, and *oxaE*) are also shown in Table 1. No optimized structures of isomers *diketB*, *diketE*, *oxaC*, or *oxaD* were located in the search as all isomerized to lower energy isomers during the optimization. Together, over 1200 conformers were generated by PCModel for the different protomers of the three structural types resulting in over 400 unique conformers for the AO⁺ b₂⁺ system.

Similarly, relative free energies for low-lying conformers (< 20 kJ/mol above lowest energy structure) of the *lacB*, *lacC*, *lacD*, *lacF* AAO⁺ b₃⁺ isomers and the lowest-energy conformer of *lacA*, *oxaA*, *oxaB*, *oxaE*, *macroA*, *macroD*, and *macroF* isomers are given in Table 2. For AAO⁺ b₃⁺, no optimized structures for *lacE*, *oxaC*, *oxaD*, *oxaF*, *macroB*, *macroC*, or *macroE* isomers were located in the search due to isomerization to lower energy isomers. For the *lacC* protomer, we located structures with two different hydrogen bonding schemes. *LacC* conformers are protonated on the lactam carbonyl oxygen and have a strong hydrogen bond with the carbonyl oxygen of the neighboring Ala residue, whereas *lacC-2* conformers are still protonated on the lactam carbonyl oxygen but have a strong hydrogen bond with the carbonyl oxygen of the N-terminal Ala residue. Both of these structures are shown in Figure 2. More than 1500 PCModel conformers were initially investigated for the b₃⁺ system, resulting over 575 unique conformers.

A separate scaling factor is required for the harmonic vibrational frequencies for comparison with experimental IRMPD spectra. A NIST recommended wavelength scaling factor does not exist for B3LYP/6-31+G(d) method-basis set combination [43]. Consequently, we re-optimized the 16 overall lowest energy conformers for AO⁺ b₂⁺ (isomers *lacD*, *lacB*, or *diketA*) as well as 15 additional low-energy conformers of the other higher-energy isomers (*lacC*, *diketD*, *lacE*, *lacA*, *oxaA*, *diketC*, *oxaE*, and *oxaB*) at the B3LYP/6-31+G(d,p) level for which the recommended scale factor is (0.964) [43]. Upon

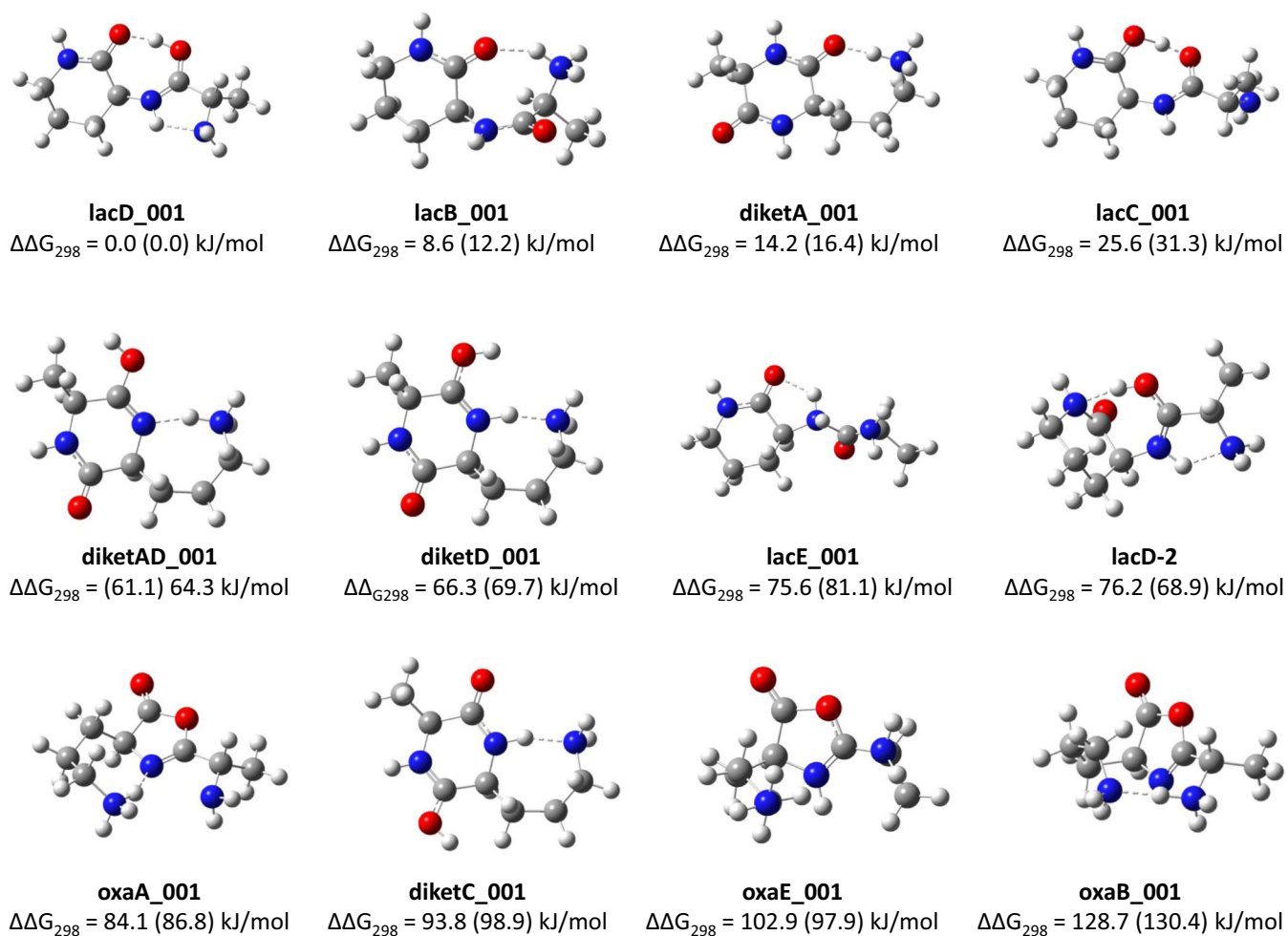


Figure 1. Lowest energy conformers for lactam (lac), diketopiperazine (diket), and oxazolone (oxa) isomers of $\text{AO}^+ \text{b}_2^+$. Different protonation sites (A–E) are shown in Scheme 1. Relative ΔG values at 298K were calculated at the B3LYP/6-311++G(d,p)//B3LYP/6-31+G(d) and B3LYP/6-31+G(d,p) (in parentheses) levels of theory

moving to the larger basis set, the *lacA* isomers, which have a strong hydrogen bond between the amide nitrogen protonation site and the backbone carbonyl oxygen, isomerized by proton transfer to *lacD* isomers. These *lacD* structures (see Figure 1) have a different hydrogen-bonding scheme ($\text{C}_{\text{backbone}}=\text{OH}^+ \cdots \text{NH}_{\text{amide}}$) than that of the lowest-energy *lacD* structures ($\text{C}_{\text{backbone}}=\text{OH}^+ \cdots \text{O}=\text{C}_{\text{lactam}}$) and will be referred to as *lacD-2* for the remainder of the manuscript. All other $\text{AO}^+ \text{b}_2^+$ isomers and all $\text{AAO}^+ \text{b}_3^+$ isomers retained structure upon switching to the larger basis set. The relative free energies of the different isomers of $\text{AO}^+ \text{b}_2^+$ at the B3LYP/6-31+G(d,p) level are shown in Figure 1 and also in Table 1. For the $\text{AAO}^+ \text{b}_3^+$ system, a total of 22 conformers were re-optimized at the B3LYP/6-31+G(d,p) level of theory. Relative free energies of the different isomers of $\text{AAO}^+ \text{b}_3^+$ at the B3LYP/6-31+G(d,p) level are shown in Figure 2 and also in Table 2. Stick spectra for all evaluated methods were broadened by a 20-cm^{-1} (baseline) Gaussian function.

In order to judge the impact of basis set and functional combination on the calculated spectra and on the relative stability of the different conformers, protomers, and isomers,

the lowest energy conformers of the *lacD*, *diketA*, and *oxaA* isomers of $\text{AO}^+ \text{b}_2^+$ were re-optimized at the M06-2X/6-311++G(d,p) [44] and $\omega\text{B97-XD}/6\text{-}311++\text{G}(\text{d},\text{p})$ [45] levels of theory to gauge the sensitivity of calculated spectra on basis set and calculation method. The relative stability order of the different isomers is the same for each calculation method: $\text{lac} < \text{diket} < \text{oxa}$, with only minor differences in relative $\Delta\Delta G$ values (within 4 kJ/mol for the diket isomers and within 1 kJ/mol for the oxa isomers relative to the global minimum lactam structure, see Table S1 of supporting information).

The spectra obtained from the different methods are also very similar (see Figures S3, S4, and S5 of supporting information). Scale factors for these spectra were chosen to line up the diagnostic C=O stretching peak in the *lacD* spectra with that of the scaled B3LYP/6-31+G(d,p) spectrum and were 0.949 for M06-2X and 0.946 for $\omega\text{B97-XD}$. Figure S3 shows that the spectra for the lowest energy lactam isomer (*lacD_001*) do not change significantly with the different approaches. The main difference being the appearance of the strongly hydrogen bonded $\text{OH}^+ \cdots \text{O}$ peak in the B3LYP spectrum at 1928 cm^{-1} . This peak appears at 1906 cm^{-1} at the M06-2x level and is predicted to lie at 2170 cm^{-1} at the

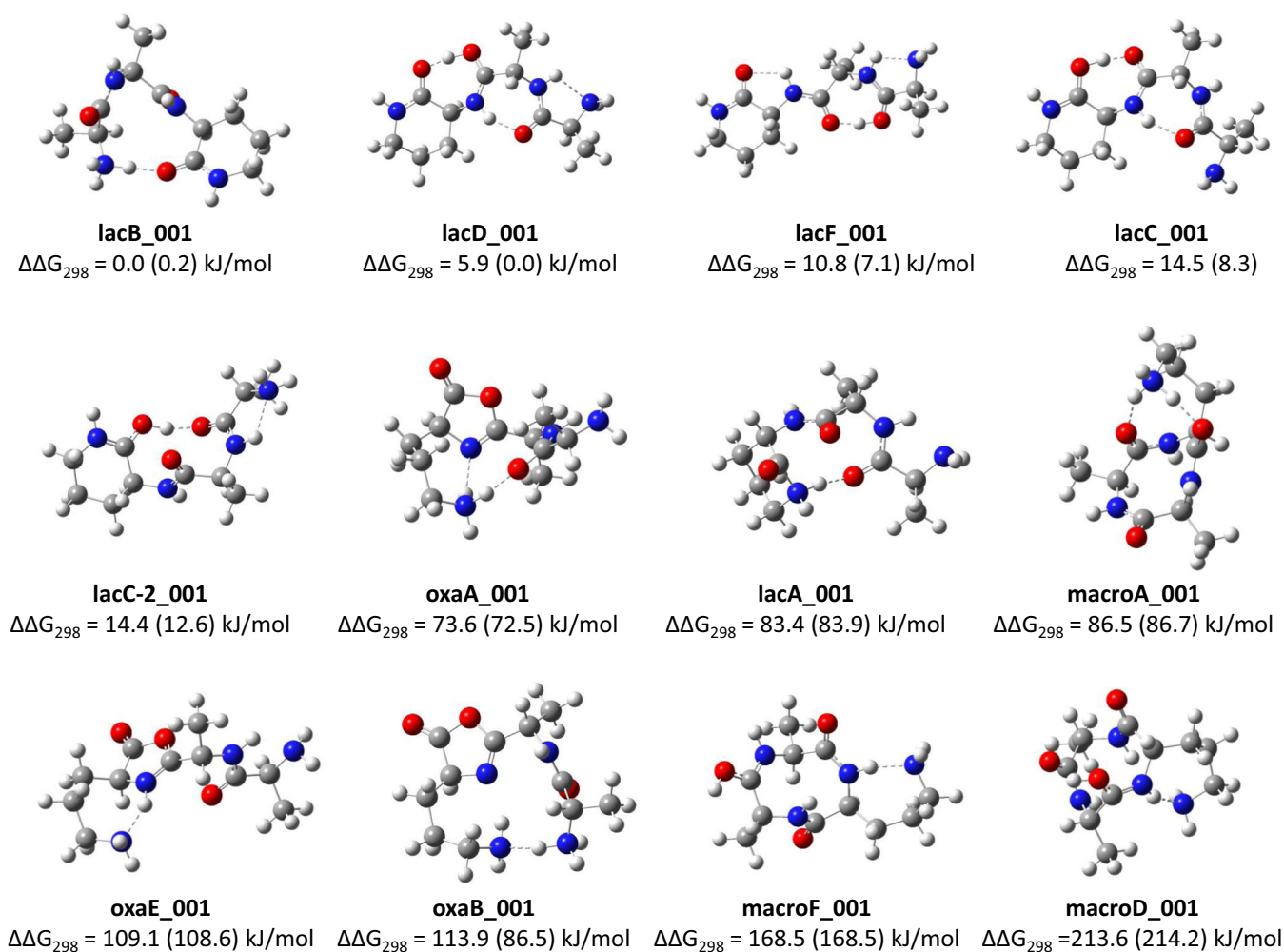


Figure 2. Lowest energy conformers for lactam (lac), macrocyclic (macro), and oxazolone (oxa) isomers of AAO⁺ b₃⁺. Different protonation sites (A–F) are shown in Scheme 1. Relative ΔG values at 298K were calculated the B3LYP/6-311++G(d,p)//B3LYP/6-31+G(d) and B3LYP/6-31+G(d,p) (in parentheses) levels of theory

Table 1. Selected Low-Energy Structures from Each Isomer Type of AO⁺. $\Delta_{298}G$ Are Reported in Hartrees. $\Delta\Delta G$ Has Been Converted to kJ/mol. ^a Calculated at B3LYP/6-311++G(d,p)//B3LYP/6-31+G(d) ^b Calculated at B3LYP/6-31+G(d,p)

| Name | Conformer | $\Delta_{298}G^a$ | $\Delta\Delta G^a$ | $\Delta_{298}G^b$ | $\Delta\Delta G^b$ |
|-------------|-----------|-------------------|--------------------|-------------------|--------------------|
| lacD_001 | lacD | -628.9839413 | 0.0 | -628.847628 | 0.0 |
| lacD_003 | lacD | -628.9813847 | 6.7 | -628.844970 | 7.0 |
| lacB_001 | lacB | -628.9806749 | 8.6 | -628.842991 | 12.2 |
| lacD_005 | lacD | -628.9789495 | 13.1 | -628.842239 | 14.2 |
| diketA_001 | diketA | -628.9785503 | 14.2 | -628.841376 | 16.4 |
| lacB_004 | lacB | -628.978362 | 14.6 | -628.841151 | 17.0 |
| diketA_003 | diketA | -628.9770828 | 18.0 | -628.839788 | 20.6 |
| lacB_007 | lacB | -628.9768285 | 18.7 | -628.839211 | 22.1 |
| diketA_005 | diketA | -628.9763434 | 19.9 | -628.838367 | 23.4 |
| diketA_007 | diketA | -628.9754819 | 22.2 | -628.838367 | 24.4 |
| lacC_001 | lacC | -628.9741941 | 25.6 | -628.835700 | 31.4 |
| diketAD_001 | diketAD | -628.9606707 | 61.1 | -628.823166 | 64.3 |
| diketD_001 | diketD | -628.9586983 | 66.3 | -628.821110 | 69.7 |
| lacE_001 | lacE | -628.9551428 | 75.6 | -628.816741 | 81.1 |
| lacD-2_001 | lacD-2 | -628.9549317 | 76.2 | -628.821409 | 68.9 |
| oxaA_001 | oxaA | -628.9518923 | 84.1 | -628.814568 | 86.8 |
| diketC_001 | diketC | -628.9482096 | 93.8 | -628.809961 | 98.9 |
| oxaE_001 | oxaE | -628.9447333 | 102.9 | -628.810342 | 97.9 |
| oxaB_001 | oxaB | -628.9349033 | 128.7 | -628.797979 | 130.4 |

ω B97-XD level and is therefore absent in the figure. This mode involves a hydrogen-bonded hydrogen and it is not surprising that the methods treat this mode differently due to the different levels of dispersion included in the methods [44, 45]. The other, more harmonic peaks match very well across the three methods. Similar agreement is seen in the calculated spectra for the lowest energy isomer of the diketopiperazine (*diketA_001*) as shown in Figure S4. The harmonic C=O stretching frequencies at 1726 cm⁻¹ and 1633 cm⁻¹ in the B3LYP spectra match reasonably well with those in spectra from the other two methods. The peaks involving the strongly hydrogen-bonded NH₃⁺ hydrogen atom again shift with method. Finally, Figure S5 shows that for the lowest energy oxazolone isomer (*oxaE*), the calculated spectra match quite well. All three methods predict a strong C=O stretching band above 1850 cm⁻¹ which eliminates the oxazolone as a possible structure for the AO⁺ b₂⁺ ion (see below). Given the significant increase in computational cost for the ω B97-XD and M06-2X triple zeta calculations and the similarity in the scaled spectra, we present only comparisons to the B3LYP/6-31+G(d,p)-derived spectra for the remainder of the paper.

Results and Discussion

AO⁺ b₂⁺

An IRMPD spectrum for AO⁺ b₂⁺ was obtained using the FELIX infrared free electron laser (IR-FEL) in Nijmegen, the Netherlands, coupled to a modified electrospray ionization-

Bruker AmaZon ion trap mass spectrometer [31]. Figure 3 shows the IRMPD spectra for AO⁺ b₂⁺ (*m/z* 186) from CID of protonated AOAA and for a synthesized reference AO-lac⁺ species (AO-lac⁺ = AlaOrn lactam; synthesis details in “Experimental” section and supporting information). These spectra are presented as un-normalized dissociation yields (Σ (fragments)/ Σ (fragments + precursor)) and confirm that the AO⁺ b₂⁺ fragment ion has a lactam structure. Collision-induced dissociation of the AO⁺ b₂⁺ fragment from AOAA (MS³) gives peaks at *m/z* 115 (presumably, formation of protonated 3-aminopiperidin-2-one), 141 (loss of 45 (possibly loss of ethylamine), and 169 (loss of NH₃). A representative CID spectrum is shown in Figure S6 in supporting information. Under similar conditions, the authentic lactam produces the same three fragments, though the intensity of the ammonia loss peak at *m/z* 169 increased relative to other two fragment ions (Figure S7). This difference may be attributed larger proportion of the *lacB* isomer (which is protonated on the NH₂ group, see below) in the authentic lactam population due to the difference in ion formation mechanism between the AO⁺ b₂⁺ and the AO-lac⁺ (CID of AOAA for AO⁺ b₂⁺ and ESI for the authentic lactam). IRMPD of the AO⁺ b₂⁺ fragment produced only *m/z* 141 and 115, whereas IRMPD of the authentic lactam gave all three fragment ions.

Figure 3 shows that the two IRMPD spectra match nearly exactly providing direct evidence for the lactam structure of the AO⁺ b₂⁺ fragment. Though the intensities of the various peaks vary to a small degree, which is to be expected in a

Table 2. Selected Low-Energy Structures from Each Isomer Type of AAO⁺. $\Delta_{298}G$ Are Reported in Hartrees. $\Delta\Delta G$ Has Been Converted to kJ/mol. ^a Calculated at B3LYP/6-311++G(d,p)/B3LYP/6-31+G(d) ^b Calculated at B3LYP/6-31+G(d,p)

| Name | Conformer | $\Delta_{298}G^a$ | $\Delta\Delta G^a$ | $\Delta_{298}G^b$ | $\Delta\Delta G^b$ |
|------------|-----------|-------------------|--------------------|-------------------|--------------------|
| lacB_001 | lacB | -876.318697 | 0.0 | -876.125152 | 0.2 |
| lacD_001 | lacD | -876.316444 | 5.9 | -876.125240 | 0.0 |
| lacB_002 | lacB | -876.316420 | 6.0 | -876.122695 | 6.7 |
| lacB_003 | lacB | -876.316160 | 6.7 | -876.122529 | 7.1 |
| lacB_005 | lacB | -876.314950 | 9.8 | -876.121300 | 10.3 |
| lacF_001 | lacF | -876.314598 | 10.8 | -876.122530 | 7.1 |
| lacF_002 | lacF | -876.313830 | 12.8 | -876.122195 | 8.0 |
| lacF_003 | lacF | -876.313434 | 13.8 | | |
| lacF_004 | lacF | -876.313432 | 13.8 | | |
| lacC-2_001 | lacC-2 | -876.313209 | 14.4 | -876.120458 | 12.6 |
| lacC_001 | lacC | -876.313161 | 14.5 | -876.122079 | 8.3 |
| lacB_007 | lacB | -876.312999 | 15.0 | | |
| lacF_005 | lacF | -876.312750 | 15.6 | | |
| lacF_006 | lacF | -876.312740 | 15.6 | | |
| lacF_007 | lacF | -876.312464 | 16.4 | | |
| lacB_011 | lacB | -876.312007 | 17.6 | | |
| lacB_012 | lacB | -876.311829 | 18.0 | | |
| lacC-2_002 | lacC-2 | -876.311535 | 18.8 | -876.118359 | 18.1 |
| lacB_014 | lacB | -876.311100 | 19.9 | | |
| lacF_008 | lacF | -876.311066 | 20.0 | | |
| lacD_002 | lacD | -876.310231 | 22.2 | -876.118514 | 17.7 |
| lacC_002 | lacC | -876.305147 | 35.6 | -876.111705 | 35.5 |
| oxaA_001 | oxaA | -876.290661 | 73.6 | -876.097624 | 72.5 |
| lacA_001 | lacA | -876.286925 | 83.4 | -876.093299 | 83.9 |
| macroA_001 | macroA | -876.285743 | 86.5 | -876.092229 | 86.7 |
| oxaE_001 | oxaE | -876.277130 | 109.1 | -876.083882 | 108.6 |
| oxaB_001 | oxaB | -876.275333 | 113.9 | -876.092307 | 86.5 |
| macroF_001 | macroF | -876.254517 | 168.5 | -876.061065 | 168.5 |
| macroD_001 | macroD | -876.237340 | 213.6 | -876.043669 | 214.2 |

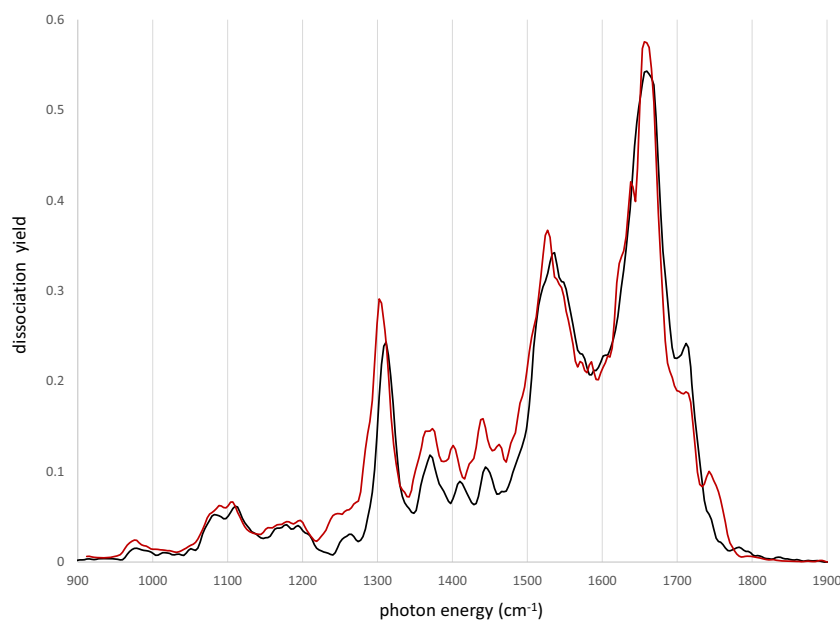


Figure 3. Normalized IRMPD spectra of b₂⁺ fragment from AOAA (black) and authentic AO-lactam (maroon)

multiphoton experiment, the positions of the peaks match nearly identically. The authentic AO⁺ lactam has a small additional peak at around 1750 cm⁻¹ that is not in the AO⁺ b₂⁺ fragment spectrum. Figure S8 of supporting information shows that this peak disappears at higher laser power (3 dB attenuation rather than 5 dB) and becomes an un-resolved shoulder. We attribute this extra peak to an additional protomer (*lacD-2*), which is present in the AO⁺ lactam population formed directly from the ESI source, but is not energetically accessible from fragmentation of AOAA to make AO⁺ b₂⁺, as discussed further below.

The IRMPD experimental results were compared with calculated spectra to provide further confirmation of the lactam structure for AO⁺ b₂⁺. The global minimum structure is a lactam protonated at the Ala carbonyl (*lacD_001*, Figure 1) with a strong hydrogen bond between the added proton and the carbonyl oxygen of the lactam. A second low-energy lactam protomer protonated at the N-terminus (*lacB_001*, Figure 1) was located 8.6 kJ/mol higher in free energy. Several additional *lacD* and *lacB* conformers were located with relative free energies in the range of 6.7–22 kJ/mol, Table 1. These species differ from the global minimum structures mainly by the conformation of the six-membered lactam ring. The lowest energy diketopiperazine structure is protonated at the Orn side chain (*diketA_001*, Figure 1) and is located 14.2 kJ/mol higher in free energy than the *lacD_001* global minimum. All other lac and diket isomers were predicted to lie at least 25 kJ/mol higher in energy than the *lacD_001* isomer. The lowest-energy oxazolone, protonated at the Orn side chain (*oxaA_001*, Figure 1), is located 84.1 kJ/mol higher in free energy. Calculated spectra for the lowest-energy conformers of the two lactams (*lacD_001* and *lacB_001*), diketopiperazine (*diketA_001*), and oxazolone (*oxaA_001*) are reproduced in Figure 4 along with

the two experimental spectra (additional spectra for higher lying isomers are shown in Figures S9a and S9b).

The experimental AO⁺ b₂⁺ fragment (black trace in Figure 4) and AO⁺ lactam (maroon trace in Figure 4) spectra both show three dominant absorptions around 1314 cm⁻¹, 1536 cm⁻¹, and 1659 cm⁻¹, several smaller peaks between 1350 and 1460 cm⁻¹, and a shoulder at 1711 cm⁻¹. In addition, the experimental AO⁺ lactam spectrum has the aforementioned peak near 1750 cm⁻¹. Comparison of the experimental spectra to the calculated spectra for the three isomers types allows us to rule out the oxazolone structure due to the lack of peaks above 1750 cm⁻¹ in the experimental spectrum. The calculated spectrum for the global minimum *lacD_001* isomer provides the closest match to the experimental spectra. The calculated *lacD_001* spectrum (purple trace in Figure 4) predicts an intense absorption at 1527 cm⁻¹ corresponding to an amide NH bend/amide C=O stretching mode that is slightly red shifted from experiment and two strong peaks at 1627 cm⁻¹ (amide C–N stretch) and 1658 cm⁻¹ (lactam C=O stretch) that match the low-energy shoulder and peak of the broad experimental feature centered around 1660 cm⁻¹. Less intense peaks are also predicted at 1310 cm⁻¹, 1366 cm⁻¹, 1411 cm⁻¹, and 1450 cm⁻¹ which match well with the experimental spectrum.

The higher-energy shoulder in the experimental spectrum at 1718 cm⁻¹ does not match the calculated spectrum for *lacD_001*. A different protomer *lacB_001* (Figure 1), which is protonated on the amino terminus and therefore has two free C=O bonding stretches, is predicted to lie only 8.6 kJ/mol higher than the *lacD_001* isomer, and should be energetically accessible in both during electrospray ionization to form AO⁺ lactam and during the fragmentation process to make AO⁺ b₂⁺. The amide C=O stretch for *lacB_001* is predicted to occur at 1703 cm⁻¹, in fair agreement with the experimental shoulder at

1718 cm⁻¹. The other two intense peaks in the calculated *lacB* spectrum at 1407 and 1650 cm⁻¹ are also in agreement with peaks in the experimental spectrum. Figure S10 displays calculated spectra for the three lowest-lying conformers of *lacD* and three lowest-lying conformers of *lacB* and shows that the spectra for the different conformers of the individual protomers do not vary much due to small changes in conformation. None of the *lacD* conformers have peaks above 1670 cm⁻¹ and all of the C=O stretches for the *lacB* conformers are between 1691 and 1704 cm⁻¹. Shifts of this magnitude (~14 cm⁻¹) are common between harmonic oscillator-based theoretical spectra and experimental spectra and can arise from anharmonicity in the vibrational mode and effects from the multiple-photon nature of the experiment [46, 47]. Given the fact that the authentic lactam shows a similar peak at 1718 cm⁻¹, we tentatively assign the shoulder at 1718 cm⁻¹ as the C=O stretch of the *lacB_001*.

The calculated spectrum for the *diketA_001* isomer (structure in Figure 1), which lies 14 kJ/mol above the *lacD* isomer and is protonated on the Orn side chain, shows a strong peak at 1727 cm⁻¹ corresponding to one of the two diketopiperazine C=O stretches. However, the rest of the calculated spectrum does not fit as well with the experimental data as the lactam spectra do. Figure S11 shows the normalized experimental AO⁺ b₂⁺ spectrum and the normalized *diketA* spectrum on the same scale and one

can see that the spectrum is not a good fit. In addition, diketopiperazine formation is dis-favored on energetic grounds. In this system, the lowest energy diketopiperazine ion is only 14 kJ/mol higher in energy than the lowest energy lactam isomer. Assuming that the dissociation time is long enough for the AOAA⁺ system to sample the relevant oxa/diket/lactam forming channels, the barriers to formation will dictate the observed products, according to the Curtin Hammett principle [48–50]. Since formation of the *diket* isomer requires a high-energy trans-cis isomerization and formation of the lactam does not (the Orn side chain contains only single bonds), the barrier for lactam formation should be lower than that for diketopiperazine formation. Given the energetic requirements of trans-cis isomerization for diketopiperazine formation and the fact that the AO⁺ b₂⁺ fragment spectrum matches so well with the spectrum for the authentic AO⁺-lac, we are confident that the AO⁺ b₂⁺ fragment ion is a mixture of *lacD* and *lacB* isomers, possibly with multiple different conformers of each present in the mixture.

As mentioned earlier, the experimental spectrum for the authentic lactam has an extra peak at 1750 cm⁻¹. Figure 5 shows a calculated spectrum for a different conformer of *lacD* in which the lactam is protonated on the backbone carbonyl atom, but instead of forming a hydrogen bond with the lactam carbonyl oxygen, the proton forms a hydrogen bond

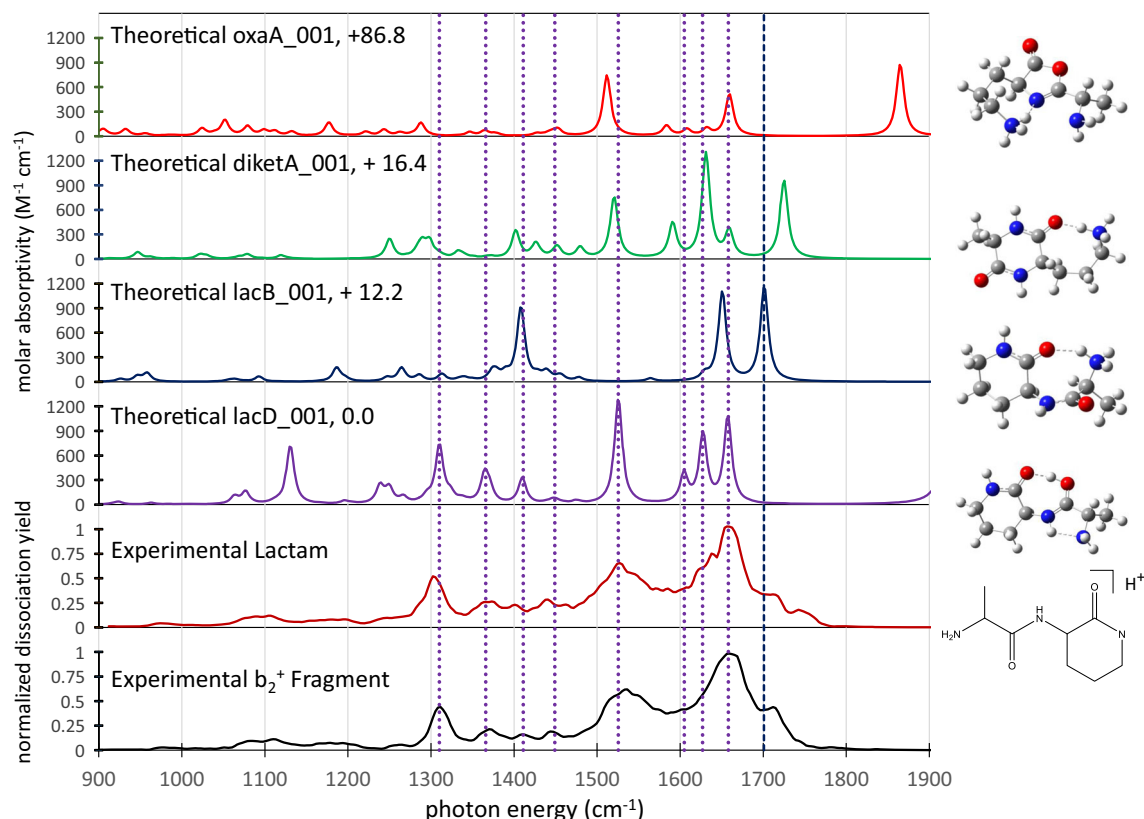


Figure 4. Overlay of the AO⁺ b₂⁺ fragment (black) and synthesized AO-lac⁺ (maroon) IRMPD spectra with the calculated spectra for *lacD_001* (purple), *lacB_001* (dark blue), *diketA_001* (green), and *oxaA_001* (red). Relative 298 K free energies in kJ/mol calculated at the B3LYP/6-31+G(d,p) level are listed for the four isomers. Dashed lines indicate the positions of diagnostic peaks from the calculated spectra. From left to right, 1310 cm⁻¹ (*lacD*), 1366 cm⁻¹ (*lacD*), 1411 cm⁻¹ (*lacD*), 1450 cm⁻¹ (*lacD*), 1527 cm⁻¹ (*lacD*), 1604 cm⁻¹ (*lacD*), 1627 cm⁻¹ (*lacD*), 1658 cm⁻¹ (*lacD*), 1703 cm⁻¹ (*lacB*)

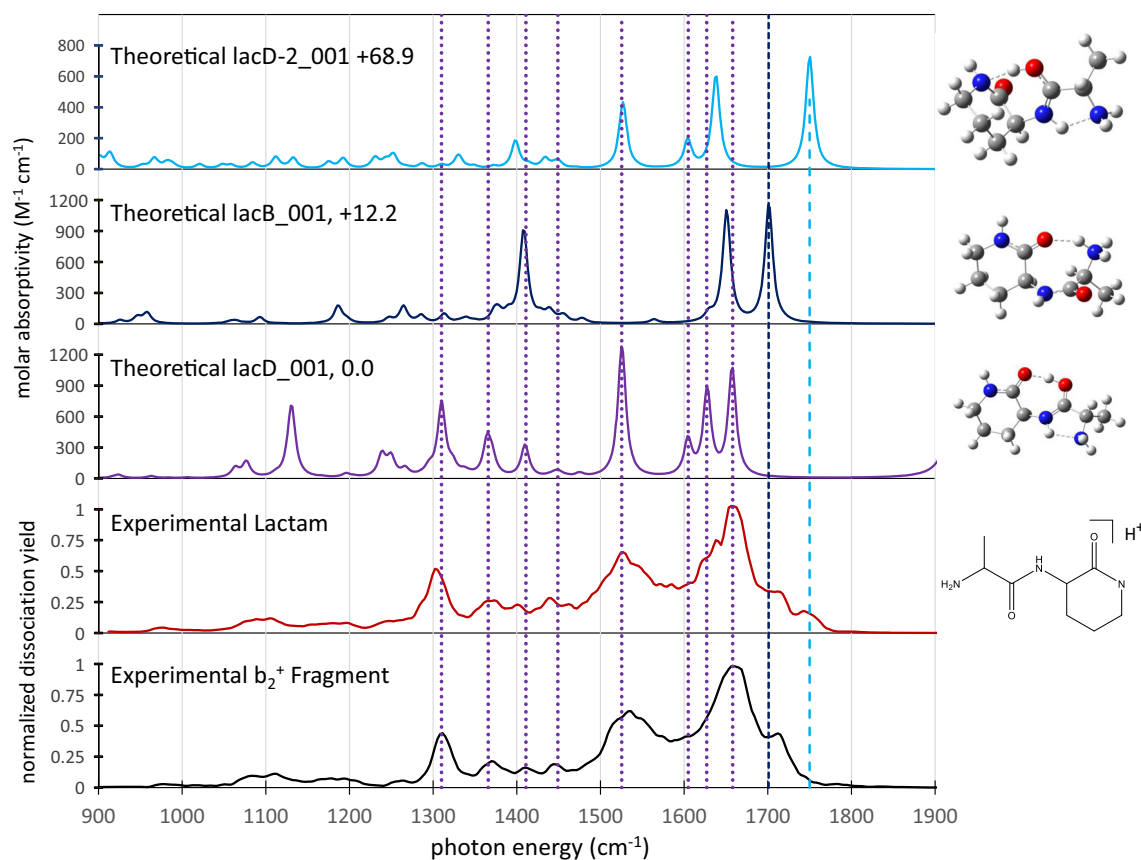


Figure 5. Overlay of the synthesized AO-lac⁺ (black) and the AO⁺ b₂⁺ fragment (maroon) IRMPD spectra with the calculated spectra of **lacD_001** (purple), **lacB_001** (dark blue), and **lacD-2_001** (light blue). Relative 298 K free energies in kJ/mol calculated at the B3LYP/6-31+G(d,p) level are listed for the three isomers. Dashed lines indicate the positions of diagnostic peaks from the calculated spectra from left to right, 1310 cm⁻¹ (**lacD**), 1366 cm⁻¹ (**lacD**), 1411 cm⁻¹ (**lacD**), 1450 cm⁻¹ (**lacD**), 1527 cm⁻¹ (**lacD**), 1604 cm⁻¹ (**lacD**), 1627 cm⁻¹ (**lacD**), 1658 cm⁻¹ (**lacD**), 1703 cm⁻¹ (**lacB**), and 1750 cm⁻¹ (**lacD-2**)

with the nitrogen atom in the lactam ring (see Figure 1 for structure). As mentioned in the theoretical procedures section, at the B3LYP/6-31+G(d) level of theory, the proton is actually formally on the lactam nitrogen (**lacA**). However, including polarization functions on the hydrogen atoms causes the **lacA** isomers to proton transfer to the backbone carbonyl oxygen. We are calling this conformer **lacD-2** and by changing the hydrogen bonding arrangement, the carbonyl oxygen atom of the lactam is no longer involved in hydrogen bonding and the C=O stretch shifts to 1750 cm⁻¹, in near perfect agreement with the peak in the experimental AO⁺-lac spectrum. This conformer lies ~65 kJ/mol higher in energy than the **lacD** conformers with OH⁺---O hydrogen bonding motif, though the protonation site is the same. This conformer could be kinetically trapped during the ESI process for AO⁺-lac, but energetically inaccessible during fragmentation of AOAA, explaining its absence in the AO⁺ b₂⁺ fragment spectrum.

AAO⁺ b₃⁺

An IRMPD spectrum of AAO⁺ b₃⁺ (*m/z* 257), shown in Figure 6, was obtained at CLIO using the IR-FEL coupled to a modified electrospray ionization-Bruker Esquire ion trap

mass spectrometer [32, 33]. CID of AAO⁺ b₃⁺ gives peaks at *m/z* 115 (again, presumably protonated 3-aminopiperidin-2-one), 186 (b₂⁺), and 239 (loss of H₂O) as shown in Figure S12. Only fragments with *m/z* 239 and 115 were seen in the IRMPD spectrum. Calculations at the B3LYP/6-311++G(d,p)//B3LYP/6-31+G(d) level predict that the lowest energy AAO⁺ structure is a lactam protonated at the N-terminus (**lacB_001**). Another low energy lactam structure protonated at the second Ala carbonyl oxygen (**lacD_001**) was located only 5.9 kJ/mol higher in free energy. Upon re-optimizing the geometries at the B3LYP/6-31+G(d,p) level of theory, these two isomers become nearly isoenergetic, with **lacD_001** being 0.2 kJ/mol more stable than the **lacB_001** isomer. Two additional lactam isomers, **lacF_001**, protonated on the first Ala carbonyl oxygen, and **lacC_001**, protonated on the lactam carbonyl, were predicted to lie 7.0 and 8.3 kJ/mol above the **lacD_001** structure at the B3LYP/6-31+G(d,p) level. In the **lacC_001** isomer, the proton on the lactam carbonyl oxygen forms a strong hydrogen bond with the carbonyl of the second Ala residue (site D) as mentioned earlier, we also located a second **lacC** isomer type still protonated on the lactam carbonyl group, but now hydrogen bonded to the carbonyl oxygen of the first Ala residue, **lacC-2_001**, which lies

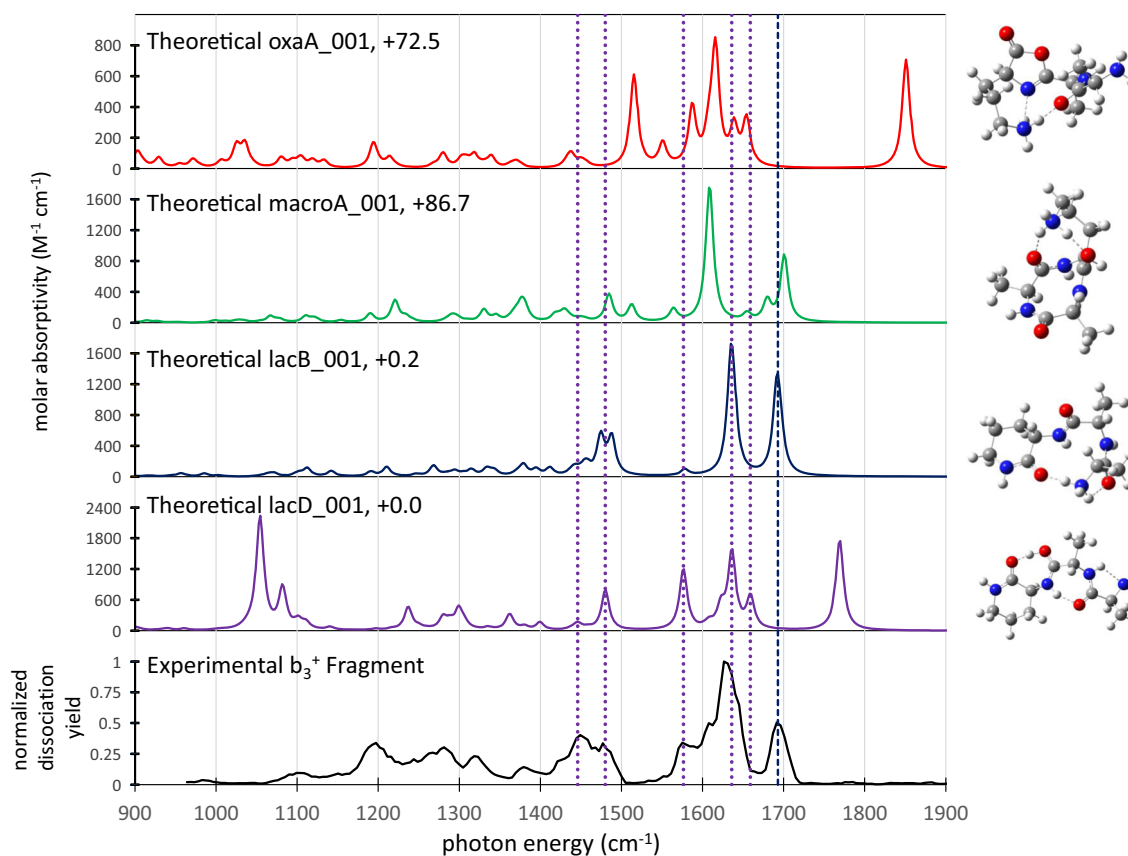


Figure 6. Experimental IRMPD spectrum for the AAO⁺ b₃⁺ fragment as compared with the calculated spectra of **lacD_001** (purple), **lacB_001** (blue), **macroA_001** (green), and **oxaA_001** (red). Relative 298 K free energies in kJ/mol calculated at the B3LYP/6-31+G(d,p) level are listed for the four isomers. Dashed lines indicate the positions of diagnostic peaks from the calculated spectra. From left to right, 1446 cm⁻¹ (**lacD**), 1480 cm⁻¹ (**lacD**), 1577 cm⁻¹ (**lacD**), 1636 cm⁻¹ (**lacD**), 1659 cm⁻¹ (**lacD**), and 1693 cm⁻¹ (**lacB**)

12.6 kJ/mol above the **lacD** isomer. The lowest-energy oxazolone structure is protonated at the Orn side chain (**-oxaA_001**) and is located 72.5 kJ/mol higher in free energy. The additional amino acid residue in this b-ion system changes the diketopiperazine structure (6-membered ring) to a macrocycle structure (9-membered ring), which also requires a trans-cis isomerization to form. The lowest-energy macrocycle structure is protonated at the Orn side chain (**macroA_001**) and located 83.9 kJ/mol higher in free energy.

Analogous to the AO⁺ b₂⁺ results, the calculated spectra for the lactam isomers provide the closest match to the experimental AAO⁺ b₃⁺ fragment spectrum, as shown in Figure 6 (additional spectra for other low-energy lactam conformers are shown in Figure S13 a and calculated spectra for the lowest-energy conformers of all the higher-energy lactam, macro, and oxa isomers are shown in Figure S13b). The experimental spectrum is characterized by a high-intensity absorption at 1626 cm⁻¹, a medium intensity absorption at 1691 cm⁻¹, and several lower intensity bands between 1200 and 1500 cm⁻¹. As with AO⁺ b₂⁺, the oxazolone form of AAO⁺ b₃⁺ can be ruled out due to the lack of peaks in the experimental spectrum above 1800 cm⁻¹.

The calculated spectra for the lactam isomers match the experimental spectrum much better than that of the oxazolone. The calculated spectrum for the **lacD_001** (Figure 6, purple trace)

isomer has a strong peak at 1635 cm⁻¹ that matches well with the large peak in the experimental spectrum. This mode is predicted to be a combination of the C=O stretch in the backbone (Ala₁) along with motion of the Ala₂ C=O and Ala₂ C–N stretches. Additional medium strength peaks at 1577 cm⁻¹ (Ala₂ amide NH bend) and 1480 cm⁻¹ (Ala₁ amide NH bend) and a weaker predicted transition at 1446 cm⁻¹ associated with CH-bending modes match other peaks in the experimental spectrum. The two strong peaks in the predicted **lacD_001** spectrum at 1766 and 1056 cm⁻¹ arise from the different motions of the ionizing proton between the two carbonyl oxygen atoms of the lactam ring and the adjacent ala residue. These sorts of strongly hydrogen-bonded ionic X–H stretches are not commonly seen in multiphoton dissociation spectroscopy experiments due to their strongly anharmonic nature and the fact that they are significantly broadened [51, 52]. The **lacD_001** spectrum does not account for the strong peak at 1691 cm⁻¹ in the experimental spectrum. The spectrum for the nearly isoenergetic **lacB_001** isomer (Figure 6, blue trace) shows a strong peak at 1694 cm⁻¹ that arises from overlapping NH₂ bending and Ala C=O stretching modes, which match those seen in the experimental spectrum. In addition, the lactam C=O peak at 1635 in the **lacB_001** spectrum also matches the peak in the experimental spectrum at 1631 cm⁻¹. One peak in the experimental spectrum that is not accounted for by the

lacD_001 or *lacB_001* isomers is at 1200 cm⁻¹. Examining the spectra for higher-energy lactams in Figure S13 shows that a higher-lying conformer of *lacB*, *lacB_003*, which lies 7.1 kJ/mol higher in free energy than *lacD_001*, does contain a peak at this wavelength corresponding to an in-plane rocking motion of the middle carbonyl group. This peak is predicted to appear at ~1210 cm⁻¹ in the lowest energy *lacB* conformer with diminished intensity. The agreement between the experimental spectrum and the calculated spectra of the low-lying lactam isomers, strongly suggests that AAO⁺ b₃⁺ is a mixture of multiple conformers of the two different lactam isomers *lacD* and *lacB*.

The calculated spectrum for the macrocyclic AAO⁺ b₃⁺ *macroA_001* is quite similar to that of the amine protonated lactam *lacB_001*. We cannot therefore rule out an appreciable population of the macrocyclic AAO⁺ b₃⁺ ion on spectroscopic grounds. Unlike in the b₂⁺ system where the lowest energy diketopiperazine isomer is predicted to lie only 14 kJ/mol above the lactam isomer, in the b₃⁺ system, the lowest energy macrocycle is predicted to be 86 kJ/mol higher in energy than the lactam. Formation of the macrocycle still requires a trans-cis isomerization, which should push the barrier even higher than 86 kJ/mol. Energetically, it is quite unfavorable to form the macrocyclic species as compared with the lactam. Finally, an additional piece of evidence that the AAO⁺ is mostly lactam is the predominance of the *m/z* = 115 peak in the IRMPD spectrum, which corresponds to protonated 3-aminopiperidin-2-one. This peak arises from the normal b_n – y_n pathway, i.e., cleavage of the amide bond and proton transfer from the nascent b-type ion to the departing aminopiperidinone fragment. It is hard to envision such a loss from the macrocyclic species. Thus, the combination of the energetic requirements for macrocycle formation, the presence of the 115 peak in the IRMPD spectrum, and the overall better match of the calculated spectra for the *lacB/lacD* isomers, we can rule out the macrocyclic isomer of AAO⁺ b₃⁺.

Conclusion

Infrared ion spectroscopy and quantum-chemical calculations confirm that AO⁺ b₂⁺ and AAO⁺ b₃⁺ fragment ions adopt a mixture of lactam structures after dissociation. The AO⁺ b₂⁺ structure is confirmed by the nearly identical spectrum for the synthesized reference AO-lac⁺. The AAO⁺ b₃⁺ experimental data indicates a mixture of lactam isomers based on comparison with theoretical spectra, the observed IRMPD products, and energetic grounds. This is the first spectroscopic evidence of lactam b-ion structures and highlights the importance of considering side-chain effects in peptide fragmentation pathways.

Acknowledgements

The authors gratefully acknowledge the aid and expertise of the CLIO facility, P. Maître, Director. The authors also would like to thank the FELIX team for their aid and expertise. This

research was supported by NIH Grant 1R15GM116180-01 and NSF Grant CHE: 1464763

References

- Fenn, J.B., Mann, M., Meng, C.K., Wong, S.F., Whitehouse, C.M.: Electrospray ionization for mass spectrometry of large biomolecules. *Science*. **246**, 64 (1989)
- Karas, M., Hillenkamp, F.: Laser desorption ionization of proteins with molecular masses exceeding 10,000 Daltons. *Anal. Chem.* **60**, 2299 (1988)
- Tanaka, K., Waki, H., Ido, Y., Akita, S., Yoshida, Y.: Protein and polymer analysis up to M/Zx 100,000 by laser ionization time-of-flight mass spectrometry. *Rapid Commun. Mass Spectrom.* **2**, 151 (1988)
- Paizs, B., Suhai, S.: Fragmentation pathways of protonated peptides. *Mass Spectrom. Rev.* **24**, 508 (2005)
- Smith, L.L., Herrmann, K.A., Wysocki, V.H.: Investigation of gas phase ion structure for proline-containing b(2) ion. *J. Am. Soc. Mass Spectrom.* **17**, 20 (2006)
- Yoon, S.H., Chamot-Rooke, J., Perkins, B.R., Hilderbrand, A.E., Poutsma, J.C., Wysocki, V.H.: IRMPD spectroscopy shows that AGG forms an oxazolone b₂⁺ ion. *J. Am. Chem. Soc.* **130**, 17644 (2008)
- Oomens, J., Young, S., Molesworth, S., van Stipdonk, M.: Spectroscopic evidence for an oxazolone structure of the b(2) fragment ion from protonated tri-alanine. *J. Am. Soc. Mass Spectrom.* **20**, 334 (2009)
- Bythell, B.J., Somogyi, A., Paizs, B.: What is the structure of b2 ions generated from doubly protonated tryptic peptides? *J. Am. Soc. Mass Spectrom.* **20**, 618 (2009)
- Perkins, B. R.; Chamot-Rooke, J.; Yoon, S. H.; Gucinski, A. C.; Somogyi, A.; Wysocki, V. H. Evidence of diketopiperazine and oxazolone structures for HA b₂⁺ ion. *J. Am. Chem. Soc.* **2009**, *131*, 17528
- Chen, X., Yu, L., Steill, J.D., Oomens, J., Polfer, N.C.: Effect of peptide fragment size on the propensity of cyclization in collision-induced dissociation: oligoglycine b2-b8. *J. Am. Chem. Soc.* **131**, 18272 (2009)
- Gucinski, A.C., Chamot-Rooke, J., Nicol, E., Somogyi, A., Wysocki, V.H.: Structural influences on preferential oxazolone versus diketopiperazine b₂⁺ ion formation for histidine analogue-containing peptides. *J. Phys. Chem. A*. **116**, 4296 (2012)
- Kullman, M.J., Molesworth, S., Berden, G., Oomens, J., Van Stipdonk, M.: IRMPD spectroscopy b₂ ions from protonated tripeptides with 4-aminomethyl benzoic acid residues. *Int. J. Mass Spectrom.* **316-318**, 174 (2012)
- Armentrout, P.B., Clark, A.: The simplest b₂⁺ ion: determining its structure from its energetics by a direct comparison of the threshold collision-induced dissociation of protonated oxazolone and diketopiperazine. *Int. J. Mass Spectrom.* **316-318**, 182 (2012)
- Bernier, M.C., Paizs, B., Wysocki, V.H.: Influence of a gamma amino acid on the structures and reactivity of peptide a₃ ions. *Int. J. Mass Spectrom.* **316-318**, 259 (2012)
- Gucinski, A.C., Chamot-Rooke, J., Steinmetz, V., Somogyi, A., Wysocki, V.H.: Influence of N-terminal residue composition on the structure of proline-containing b₂⁺ ions. *J. Phys. Chem. A*. **117**, 1291 (2013)
- Morrison, L.J., Chamot-Rooke, J., Wysocki, V.H.: IR action spectroscopy shows competitive oxazolone and diketopiperazine formation in peptides depends on peptide length and identity of terminal residue in the departing fragment. *Analyst*. **139**, 2137 (2014)
- Karaca, S., Atik, A.E., Elmaci, N., Yalcin, T.: Gas-phase structures and proton affinities of N-terminal proline containing b2+ ions from protonated model peptides. *Int. J. Mass Spectrom.* **393**, 1 (2015)
- Bernier, M.C., Chamot-Rooke, J., Wysocki, V.H.: R vs. S fluoroproline ring substitution: *trans/cis* effects on the formation of b₂ ions in gas-phase peptide fragmentation. *Phys. Chem. Chem. Phys.* **18**, 2202 (2016)
- Grzetic, J., Oomens, J.: Spectroscopic identification of cyclic imide b₂-ions from peptides containing Gln and Asn residues. *J. Am. Soc. Mass Spectrom.* **24**, 1228 (2013)
- Martens, J.K., Grzetic, J., Berden, G., Oomens, J.: Gas-phase conformations of small polyprolines and their fragment ions by IRMPD spectroscopy. *Int. J. Mass Spectrom.* **377**, 179 (2015)
- Poutsma, J.C., Martens, J.K., Oomens, J., Maitre, P., Steinmetz, V., Bernier, M., Jia, M., Wysocki, V.H.: Infrared multiple-photon dissociation action spectroscopy of the b₂⁺ ion from PPG: evidence of third residue affecting b₂⁺ fragment structure. *J. Am. Soc. Mass Spectrom.* **28**, 1482 (2017)

22. Grzetic, J., Oomens, J.: Effect of the Asn side chain on the dissociation of deprotonated peptides elucidated by IRMPD spectroscopy. *Int. J. Mass Spectrom.* **354-355**, 70 (2013)
23. Nelson, C.R., Abutokaiyah, M.T., Harrison, A.G., Bythell, B.J.: Proton mobility in b₂ ion formation and fragmentation reactions of histidine-containing peptides. *J. Am. Soc. Mass Spectrom.* **27**, 487 (2015)
24. Bythell, B.J., Csonka, I.P., Suhai, S., Barofsky, D.F., Paizs, B.: Gas-phase structure and fragmentation pathways of singly protonated peptides with N-terminal arginine. *J. Phys. Chem. B.* **114**, 15092 (2010)
25. McGee, W.M., McLuckey, S.A.: The ornithine effect in peptide cation dissociation. *J. Mass Spectrom.* **48**, 856 (2013)
26. Crittenden, C.M., Parker, W.R., Jenner, Z.B., Bruns, K.A., Akin, L.D., McGhee, W.M., Ciccimaro, E., Brodbelt, J.S.: Exploitation of the ornithine effect enhances characterization of stapled and cyclic peptides. *J. Am. Soc. Mass Spectrom.* **27**, (2016)
27. Polfer, N.C., Oomens, J.: Vibrational spectroscopy of bare and solvated ionic complexes of biological relevance. *Mass Spectrom. Rev.* **28**, 468 (2009)
28. Chan, W.C., White, P.D.: *Fmoc solid phase peptide synthesis: a practical approach*. Oxford University Press, New York (2000)
29. Amblard, M., Fehrentz, J.-A., Subra, G.: Methods and protocols of modern solid phase peptide synthesis. *Mol. Biotechnol.* **33**, 239 (2006)
30. Martens, J.; Grzetic, J.; Berden, G.; Oomens, J. Structural identification of electron transfer dissociation products in mass spectrometry using infrared ion spectroscopy *Nat. Commun.* **2016**, *7*, 11754
31. Martens, J.K., Berden, G., Gebhardt, C.R., Oomens, J.: Infrared ion spectroscopy in a modified quadrupole ion trap mass spectrometer at the FELIX free electron laser laboratory. *Rev. Sci. Instrum.* **87**, 103108 (2016)
32. Prazeres, R., Glotin, F., Insa, C., Jaroszynski, D.A., Ortega, J.M.: Two-colour operation of a free-electron laser and applications in the mid-infrared. *Eur. J. Mass Spectrom.* **3**, 87 (1998)
33. Aleese, L.M., Simon, A., McMahon, T.B., Ortega, J.M., Scuderi, D., Lemaire, J., Maitre, P.: Mid-IR spectroscopy of protonated leucine methyl ester performed with an FTICR or a Paul type ion-trap. *Int. J. Mass Spectrom.* **249**, 14 (2006)
34. Frisch, M. J.; Trucks, G. W.; Schlegel, H. B.; Scuseria, G. E.; Robb, M. A.; Cheeseman, J. R.; Scalmani, G.; Barone, V.; Mennucci, B.; Petersson, G. A.; Nakatsuji, H.; Caricato, M.; Li, X.; Hratchian, H. P.; Izmaylov, A. F.; Bloino, J.; Zheng, G.; Sonnenberg, J. L.; Hada, M.; Ehara, M.; Toyota, K.; Fukuda, R.; Hasegawa, J.; Ishida, M.; Nakajima, T.; Honda, Y.; Kitao, O.; Nakai, H.; Vreven, T.; Montgomery, J. A., Jr.; Peralta, J. E.; Ogliaro, F.; Bearpark, M.; Heyd, J. J.; Brothers, E.; Kudin, K. N.; Staroverov, V. N.; Kobayashi, R.; Normand, J.; Raghavachari, K.; Rendell, A.; Burant, J. C.; Iyengar, S. S.; Tomasi, J.; Cossi, M.; Rega, N.; Millam, J. M.; Klene, M.; Knox, J. E.; Cross, J. B.; Bakken, V.; Adamo, C.; Jaramillo, J.; Gomperts, R.; Stratmann, R. E.; Yazyev, O.; Austin, A. J.; Cammi, R.; Pomelli, C.; Ochterski, J. W.; Martin, R. L.; Morokuma, K.; Zakrzewski, V. G.; Voth, G. A.; Salvador, P.; Dannenberg, J. J.; Dapprich, S.; Daniels, A. D.; Farkas, Ö.; Foresman, J. B.; Ortiz, J. V.; Cioslowski, J.; Fox, D. J. *Gaussian 09*, revision E.01 E. 01 Gaussian, Inc., Wallingford, CT 2013
35. PCModel Serena Software, 2006
36. Becke, A.D.: Density functional thermochemistry. III. The role of exact exchange. *J. Chem. Phys.* **98**, 5648 (1993)
37. Lee, C., Yang, W., Parr, R.G.: Development of the Colle-Salvetti correlation energy formula into a functional of the electron density. *Phys. Rev. B.* **37**, 785 (1988)
38. Scott, A.P., Radom, L.: Harmonic vibrational frequencies: an evaluation of Hartree-Fock, Moeller-Plesset, quadratic configuration interaction, density functional theory, and semiempirical scale factors. *J. Phys. Chem.* **100**, 16502 (1996)
39. Andriole, E.J., Colyer, K.E., Cornell, E., Poutsma, J.C.: Proton affinity of canavanine and canaline, oxy-analogs of arginine and ornithine, from the extended kinetic method. *J. Phys. Chem. A.* **110**, 11501 (2006)
40. Jones, C.M., Bernier, M., Carson, E., Colyer, K.E., Metz, R., Pawlow, A., Wischow, E., Webb, L., Andriole, E.J., Poutsma, J.C.: Gas-phase acidities of the 20 protein amino acids. *Int. J. Mass Spectrom.* **267**, 54 (2007)
41. Muetterties, C., Drissi Touzani, A., Hardee, I., Huynh, K.T., Poutsma, J.C.: Gas-phase acid-base properties of 1-aminocycloalkane-1-carboxylic acids from the extended kinetic method. *Int. J. Mass Spectrom.* **378**, 59 (2015)
42. Schroeder, O.E., Andriole, E.J., Carver, K.L., Poutsma, J.C.: The proton affinity of lysine analogs using the extended kinetic method. *J. Phys. Chem. A.* **108**, 326 (2004)
43. In NIST Standard Reference Database 101; Johnson III, R. D., Ed.; national institute of standards: 2018
44. Zhao, Y., Trular, D.G.: The M06 suite of density functionals for main group thermochemistry, thermochemical kinetics, noncovalent interactions, excited states, and transition elements: two new functionals and systematic testing of four M06-class functionals and 12 other functionals. *Theor. Chem. Accounts.* **120**, 215 (2008)
45. Chai, J.-D., Head-Gordon, M.: Long-range corrected hybrid density functionals with damped atom-atom dispersion corrections. *Phys. Chem. Chem. Phys.* **10**, 6615 (2008)
46. Polfer, N.C.: Infrared multiple photon dissociation spectroscopy of trapped ions. *Chem. Soc. Rev.* **40**, 2211 (2011)
47. Boles, G.C., Hightower, R.L., Coates, R.A., McNary, C.P., Berden, G., Oomens, J., Armentrout, P.B.: Experimental and theoretical investigations of infrared multiple photon dissociation spectra of aspartic acid complexes with Zn²⁺ and Cd²⁺. *J. Phys. Chem. B.* **122**, 3836 (2018)
48. Curtin, D.Y.: Stereochemical control of organic reactions. Differences in behavior of diastereomers 1. Ethane derivatives. The cis effect. *Rec. Chem. Prog.* **15**, 111 (1954)
49. Hauptert, L.J., Poutsma, J.C., Wenthold, P.G.: The Curtin-Hammett principle in mass spectrometry. *Acc. Chem. Res.* **42**, 1480 (2009)
50. Armentrout, P.B., Heaton, A.L.: Thermodynamics and mechanisms of protonated Diglycine decomposition: a computational study. *J. Am. Soc. Mass Spectrom.* **23**, 621 (2012)
51. Roscioli, J.R., R., M. L., Johnson, M.A.: Quantum structure of the intermolecular proton bond. *Science.* **316**, 249 (2007)
52. Dit Fouque, K.J., Lavanant, H., Zirah, S., Steinmetz, V., Rebuffat, S., Maitre, P., Afonso, C.: IRMPD spectroscopy: evidence of hydrogen bonding in the gas phase conformations of lasso peptides and their branched-cyclotopoisomers. *J. Phys. Chem. A.* **2016**, *120*, (2016)